CHEMISTRY OF MATERIALS

Article

pubs.acs.org/cm

Charge Transfer in Molecular Complexes with 2,3,5,6-Tetrafluoro-7,7,8,8-tetracyanoquinodimethane (F_4-TCNQ): A Density Functional Theory Study

Lingyun Zhu, Eung-Gun Kim,*[,†] Yuanping Yi, and Jean-Luc Brédas*[,‡]

School of Chemistry and Biochemistry and Center for Organic Photonics and Electronics, Georgia Institute of Technology, Atlanta, Georgia 30332-0400, United States

Supporting Information

ABSTRACT: Molecular doping is a charge-transfer process intended to improve the electrical properties of organic semiconductors and the efficiency of organic electronic devices, by incorporation of a complex-forming, strong molecular electron acceptor or donor. Using density functional theory methods with dispersion corrections, we seek to monitor charge transfer and estimate its amount via calculations of experimental observables. With 2,3,5,6-tetrafluoro-7,7,8,8-tetracyanoquinodimethane (F_4-TCNQ) as a *p*-dopant (electron acceptor) and an array of π-conjugated molecules as hole-transport materials (donors), the amount of charge transfer is seen to be a non-monotonic function of the offset defined by the donor ionization potential (IP) and the acceptor electron affinity (EA), IP − |EA|. Interestingly, a well-defined, *linear* relationship between the amount of charge transfer and IP − |EA| is obtained when the IP and EA values are adjusted to reflect intramolecular geometric changes in the final form of the complex. This study offers a straightforward way to match donor−acceptor pairs with desired doping effects and to estimate the resulting charge density in organic semiconductors.

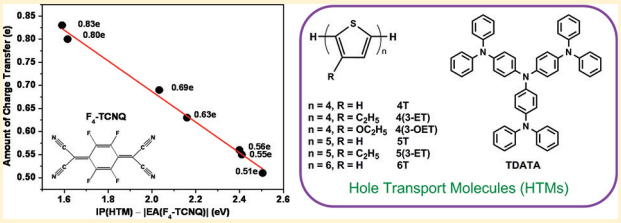

KEYWORDS: *molecular doping, charge transfer, molecular complexes, organic semiconductors, IP−EA offset, DFT*

1. INTRODUCTION

Molecular doping of organic semiconductors has become a very attractive venue for the development of efficient organic (opto)electronic devices.[1] Here, molecular doping refers to the formation of charge-transfer complexes by combining appropriate pairs of electron donors and acceptors, with an aim to achieve improvement on electrical properties such as charge injection and conductivity.[1−3] In *p*-type doping, an electron acceptor acts as the dopant, and in *n*-type doping, an electron donor does. It is commonly considered that, for efficient *p*-doping, for instance, the electron affinity (EA) of the dopant must be larger in magnitude than the ionization potential (IP) of the host material.[1]

The phenomenon of charge transfer in molecular complexes is a well-studied subject, the foundation of which was laid by Mulliken over half a century ago.[4] There are a number of factors that govern the charge transfer, a few of the most important being the donor IP−acceptor |EA| offset and various intermolecular interactions.[5,6] Successful demonstrations[1] of molecular doping as an effective tool to improve the performance of organic semiconductor devices have renewed interest in charge transfer, now in a different context. For example, by systematically varying the IP of the host material, using various conjugated polymers, with respect to the EA of a *p*-dopant, Yim et al. showed[7] that the smaller the IP of the polymer, the more effective the doping is in increasing the electrical conductivity. Also, Avilov et al. investigated[8] theoretically the role of charge transfer in the formation of interface dipoles at organic−organic interfaces.

How the IP−|EA| offset affects the amount of charge transfer depends critically on the strength of electronic coupling between the donor and the acceptor. In the weak coupling limit, charge transfer does not take place until the offset reaches a threshold value, at which one electron is transferred;[8,9] because of its biradical nature, the ground-state electronic structure of such a charge-transfer complex would require a multi-configurational description.[8] However, with increasing electronic coupling, this step-function-like transition is smeared and takes the form of a stretched S-shape, and continuous partial charge transfer is allowed.[9] When a large amount of partial charge transfer is involved, as in molecular doping, single-reference methods such as those based on the current formulation of density functional theory (DFT) become a suitable alternative because these methods inherently predict a continuous transfer of partial charge.[9]

Here, we investigate *p*-doping by a very strong electron acceptor, of a number of hole-transport molecules with varying IPs, using dispersion-corrected density functional

Received: June 23, 2011
Revised: October 17, 2011
Published: November 8, 2011

theory (DFT-D) methods. The electron acceptor we have chosen is 2,3,5,6-tetrafluoro-7,7,8,8-tetracyanoquinodimethane (F_4-TCNQ), a widely used *p*-dopant with a very high EA[10−17] (see Figure 1 for the chemical structures). We explore how the

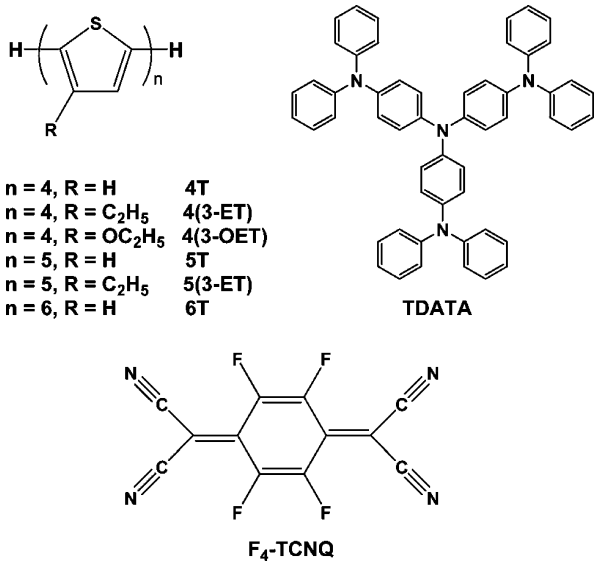

Figure 1. Chemical structures of oligothiophene derivatives and 4,4′,4″-tris(*N*,*N*-diphenylamino)triphenylamine (TDATA), as hole-transport molecules, and 2,3,5,6-tetrafluoro-7,7,8,8-tetracyanoquinodimethane (F_4-TCNQ), as a *p*-dopant.

amount of charge transfer is manifested through experimental observables, such as bond lengths, vibrational frequencies, and the IP−|EA| offset, in the limits of strong electronic coupling and high partial charge transfer. In doing so, we validate our theoretical approach by comparing the results against a variety of experimental data.

2. METHODOLOGY

The geometries of the charge-transfer complexes were optimized by using DFT methods with the B3LYP functional and Grimme's dispersion corrections[18,19] (B3LYP-D), and the 6-31+G(d) basis set. The dispersion corrections, made at an empirical level, add little computational cost. Initial guesses for the complex geometry were constructed by varying intermolecular distance and orientation and were subjected to geometry optimization without any geometrical constraints. The geometries of the individual molecules in the neutral and charged states were optimized at the B3LYP/6-31+G(d) level. The crystal structure of pristine F_4-TCNQ was optimized at the B3LYP/6-31G(d) level with a uniform Monkhorst−Pack *k*-point mesh of 4 × 6 × 6, in which the atomic positions in the unit cell were relaxed, while the cell parameters were kept fixed at the experimental values. For comparison, some of the calculations were also carried out at the RI-MP2/aug-cc-pVDZ level (resolution of the identity, second-order Møller−Plesset perturbation theory with the aug-cc-pVDZ basis set). RI methods are based on the approximate evaluation of the four-centered two-electron integrals by using three-centered integrals, which makes the calculation considerably faster.[20]

Harmonic vibrational frequencies and intensities were calculated (at the Γ-point only in the case of the crystal). Calculated frequencies were scaled by a factor of 0.9614, which has been shown to reproduce the experimental frequencies very well.[21] The simulation of IR spectra was carried out by a Lorentzian convolution with a full width at half maximum (fwhm) of 4.5 or 8 cm^{-1}.

A fragment orbital approach,[22] in combination with a basis set orthogonalization procedure,[23] was used to evaluate the effective transfer integral between the donor and the acceptor in the complex. These calculations were performed at the B3LYP/6-31+G(d) level.

Time-dependent density functional theory (TDDFT) was used at the B3LYP/6-31+G(d) level on the optimized ground-state geometries to calculate the excitation energy and oscillator strength for electronic transitions from the ground to excited states. The simulated absorption spectra were then obtained as a Gaussian convolution with a fwhm of 0.1 eV. The natural transition orbital (NTO) approach,[24,25] which provides a simple orbital interpretation of excitation, was used to analyze and visualize the electronic excitations.

The *TURBOMOLE 6.0*[26] and *CRYSTAL06*[27] packages were used for molecular and crystal calculations, respectively, with the exception of the transfer integrals, for which the *Gaussian 03* package was used.[28] All presented results are those of the molecular calculations unless labeled appropriately with "crystal."

3. RESULTS AND DISCUSSION

3.1. Dispersion Interactions and Intermolecular Geometry. The London dispersion forces represent an attractive interaction arising from fluctuating charge distributions,[29] which is essential to describe the properties of many molecular complexes in general.[5,18,29] In quantum-mechanical terms, the dispersion interaction is a dynamic, long-range electron correlation effect that is not captured by popular density functionals.[30] The DFT-D approach adds a simple empirical dispersion correction to the DFT calculation,[18,19,31−35] and has been shown to provide a very efficient means to accurately calculate binding energies[36,37] and geometries.[38] In the following example of *p*-doping of quaterthiophene (4T) by F_4-TCNQ, we illustrate the impact of having a proper description of the dispersion interaction on the intermolecular structure, and thus the amount of charge transfer, of a charge-transfer complex.

The F_4-TCNQ/4T pair is a particularly relevant model system for studying the doping process because one of the first successful demonstrations of doping polymeric hole-transport layers using F_4-TCNQ was made in the case of poly(3-hexylthiophene) (P3HT),[7,39] which one can effectively represent by 4T. Calculations at the B3LYP-D/6-31+G(d) level, where F_4-TCNQ is moved along the long molecular axis of 4T in a cofacial arrangement, lead to three energy-minimum intermolecular geometries (see Figure 2).

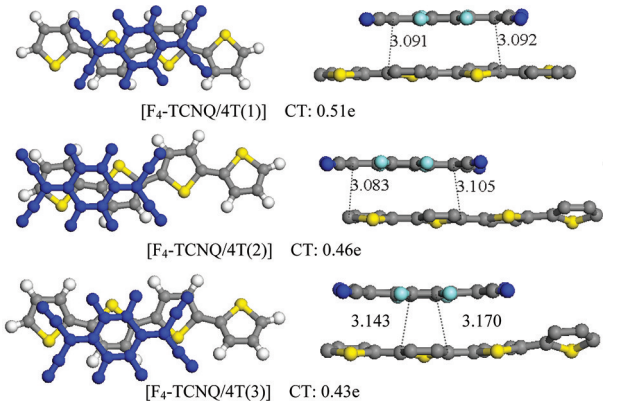

Figure 2. B3LYP-D/6-31+G(d)-optimized geometries of the F_4-TCNQ/4T complex at three energy minima (top view, left; side view, right). Interatomic distances between two molecules (in Å) and the amount of charge transfer, CT, are shown. For clarity, hydrogen atoms are not shown in the side views.

The lowest energy geometry, denoted here by F_4-TCNQ/4T(1), is found when the F_4-TCNQ center is located above the

dx.doi.org/10.1021/cm201798x|*Chem. Mater.* 2011, 23, 5149−5159

bond connecting the two inner thiophene rings; the complex binding energy is calculated to be −35.6 kcal/mol. A second geometry, F_4-TCNQ/4T(2), is 3.0 kcal/mol higher in energy, and places F_4-TCNQ above the bond connecting the outer and inner thiophene rings. F_4-TCNQ/4T(3) is 5.6 kcal/mol higher than the first geometry and finds the dopant above one of the inner thiophene rings. The F_4-TCNQ moiety, fully planar as an isolated molecule, is now distorted and asymmetric in all three optimized complexes. The shortest interatomic distance between two molecules is in the range of 3.08−3.17 Å. The amount of charge transfer increases from 0.43e to 0.51e, with increasing stability of the formed molecular complex.

When switching off the dispersion correction to recover the standard B3LYP/6-31+G(d) methodology, we find, for F_4-TCNQ/4T(1), that there are three notable changes: (i) the intermolecular distance increases significantly from 3.09 to 3.57 Å; (ii) the intermolecular interaction energy decreases from −35.6 to −9.6 kcal/mol; and (iii) the charge transfer decreases from 0.51e to 0.36e. Additionally removing the diffuse functions from the basis set, which leads to 6-31G(d), affects only slightly the intermolecular distance (3.51 Å) and charge transfer (0.32e). The results are collected in Table 1.

Table 1. Intermolecular Distance, *d* (Å), Intermolecular Interaction Energy, Δ*E* (kcal/mol), and the Amount of Charge Transfer, CT (e), for the F_4-TCNQ/4T(1) Complex, as Calculated by DFT, DFT-D, and MP2

method[a]	*d*[b]	Δ*E*	CT
B3LYP/6-31G(d)//B3LYP/6-31G(d)	3.51	−9.2	0.32
B3LYP/6-31+G(d)//B3LYP/6-31+G(d)	3.57	−9.6	0.36
B3LYP-D/6-31+G(d)//B3LYP-D/6-31+G(d)	3.09	−35.6	0.51
		−31.0[c]	
RI-MP2/aug-cc-pVDZ//B3LYP-D/6-31+G(d)	3.09	−63.0	0.51
		−41.2[c]	
RI-MP2/aug-cc-pVDZ//RI-MP2/aug-cc-pVDZ	2.82	−73.6	0.58
		−48.0[c]	

[a]In A//B, A denotes the method to calculate Δ*E* and CT, and B denotes the method to optimize the geometry of the complex. [b]Shortest interatomic distance between two molecules. [c]Counterpoise-corrected value.

RI-MP2/aug-cc-pVDZ gives a smaller intermolecular distance of 2.82 Å and a larger interaction energy of −48.0 kcal/mol (counterpoise-corrected) than B3LYP-D/6-31+G(d). This can be expected because MP2 tends to overestimate the $\pi-\pi$ interaction energy.[18,40,41] The amount of charge transfer is 0.58e; however, at the same MP2 level but using the B3LYP-D/6-31+G(d) geometry, the DFT-D value of 0.51e is recovered.

3.2. Bond Length Changes as a Quantitative Measure of Charge Transfer. The extent of the intramolecular geometric changes accompanying charge transfer is dictated by the amount of charge transfer. Information on bond length changes, as obtained by X-ray crystallography in particular, can be used to estimate the transferred amount, as shown experimentally for organic salts of TCNQ over a wide charge transfer range.[42−44]

Shown in Figure 3a is the evolution of the bond lengths of F_4-TCNQ in going from the isolated neutral state to a charge-transfer complex to the isolated anionic state. As expected, the bond lengths of the complex fall between those of the neutral and completely ionic species, an indication that the two

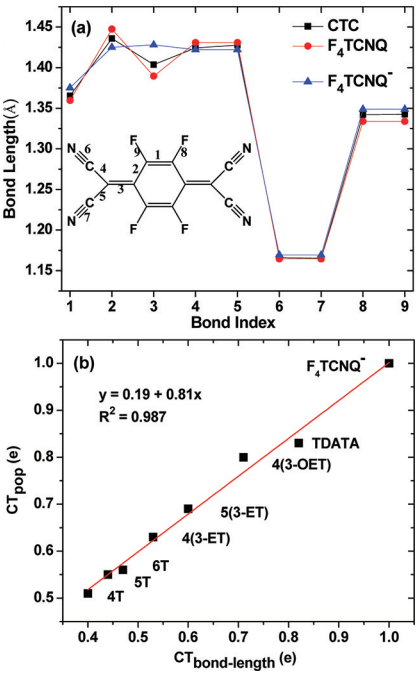

Figure 3. Charge transfer as manifested in bond-length changes of F_4-TCNQ. (a) Calculated bond lengths for the isolated neutral molecule, the charge-transfer complex with 4T (CTC), and the mono-anion. (b) Comparison of the charge transfer estimated from bond-length changes ($CT_{bond\ length}$) using eq 1, with the charge transfer calculated directly from the natural population analysis (CT_{pop}), for all complexes with various donors.

molecules in the complex have exchanged a partial charge. To extract the amount of charge transfer ρ from the calculated bond lengths of F_4-TCNQ, we use the method proposed by Kistenmacher et al.[42] for TCNQ:

$$\rho = -\frac{\alpha_{CT} - \alpha_0}{\alpha_{-1} - \alpha_0} \quad (1)$$

with $\alpha_i = l_3/(l_2+l_4)$, where l is the bond length, and subscript i = 0, −1, and CT denote the neutral molecule, the anion, and the complex, respectively (see the inset of Figure 3a for the bond labeling in our case of F_4-TCNQ). This method accounts for the lengthening of a double bond (bond 3) and the shortening of two single bonds (bonds 2 and 4), all three of which represent the most notable changes. The charge transfer thus estimated from the (averaged) geometric changes is plotted in Figure 3b against the charge transfer calculated directly from the natural population analysis. The linearity of the plot confirms the relevance of eq 1, which was derived from experiment in the wide transfer range 0.2e−0.7e,[42−44] and provides strong evidence of the suitability of our theoretical method, especially in a high charge transfer regime.

Inspection of the fully optimized complex geometries indicates that the *inter*molecular distance remains unchanged among different complexes (or with increasing amount of charge transfer) and thus confirms the validity of the frozen geometry approximation commonly adopted for the intermolecular distance.[8,9] Such an approximation, however, does not hold for the *intra*molecular geometry; it is clear from Figure 3a that constricting the intramolecular geometry would underestimate the amount of charge transfer to an extent that grows with increasing amount of charge transfer.

dx.doi.org/10.1021/cm201798x|*Chem. Mater.* 2011, 23, 5149−5159

3.3. Vibrational Frequency Shifts as a Quantitative Measure of Charge Transfer. Vibrational spectroscopy is an important tool for investigating the degree of ground-state charge transfer.[45−47] Stretching modes of the C≡N triple bonds in F_4-TCNQ are sensitive to charge transfer and observed in a spectral zone where no other resonance is found, making these stretching modes ideally suited for such purposes.

Isolated F_4-TCNQ is calculated to have four C≡N stretching modes with b_{3g}, b_{2u}, a_g, and b_{1u} symmetries, among which only the b_{2u} and b_{1u} modes are IR-active to give rise to a strong band at 2220 cm^{-1} and a weak band at 2239 cm^{-1}, respectively (see Figure 4 and Table 2). Experimentally, when measured in chloroform solution, a strong peak is found at 2213 cm^{-1} and a weak shoulder at around 2227 cm^{-1}.[48] In going from the isolated neutral molecule to the isolated anion, the calculated frequencies red-shift by 58 (b_{2u}) and 46 (b_{1u}) cm^{-1}. These shifts are slightly larger than the experimental values of 42 (b_{2u}) and 34 (b_{1u}) cm^{-1} for the anion in a CH_3CN solution.[49]

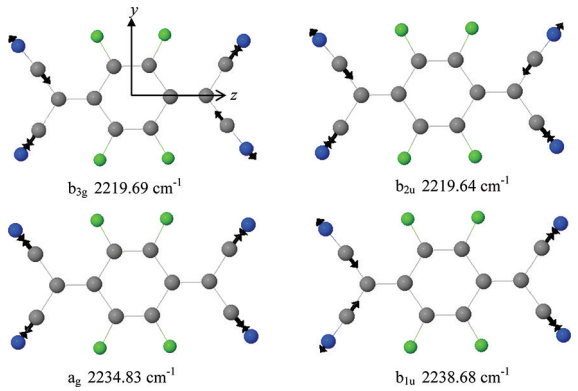

Figure 4. Normal modes of C≡N stretching in the isolated F_4-TCNQ molecule.

The frequencies of the C≡N stretching modes in the charge-transfer complexes, calculated at the B3LYP-D/6-31+G(d) level, are collected in Table 3. There are four common features among all complexes: (i) the red-shift with respect to the neutral molecule is an increasing function of charge transfer; (ii) the high-frequency b_{1u} mode has a stronger intensity than the low-frequency b_{2u} mode, which is the opposite in the isolated neutral molecule; (iii) the b_{3g} and a_g modes that are IR-inactive in the neutral molecule and remain inactive in the isolated anion are now IR-active as a result of the lower symmetry of the complex; and (iv) the intensity of the a_g mode becomes so large as to exceed that of the neighboring b_{1u} mode in some cases.

Figure 5 shows that the frequency red-shift grows approximately linearly as the charge transfer increases, in accord with the experimental observation that Bloch and coworkers[50] made among a number of TCNQ salts. The lower quality of the linearity visible in Figure 5 than what we saw in Figure 3b can be related to the fact that the C≡N stretching modes in our complexes are quite uneven, unlike those in the crystalline TCNQ salts.

The fact that the b_{1u} mode becomes stronger in intensity than the b_{2u} mode upon complex formation can be easily associated with intramolecular geometric changes, as is clear from the reversed intensities also seen in the *isolated* anion (Table 2). *Inter*molecular contributions, though less obvious, can be expected as well. We show below that the pristine crystal of F_4-TCNQ is calculated to have the reversed intensities and that the effect of the intermolecular interactions is general and not specific to those involving charge transfer. In the pristine crystal, F_4-TCNQ molecules pack into an orthorhombic lattice

Table 2. Calculated Vibrational Frequencies ω (cm^{-1}) (Scaled by 0.9614) and Intensities (km/mol) for C≡N Stretching Modes in the Isolated Neutral Molecule and Anion of F_4-TCNQ

	F_4-TCNQ		F_4-TCNQ		F_4-TCNQ		F_4-TCNQ$^-$		F_4-TCNQ$^-$	
	B3LYP/6-31G(d)		B3LYP/6-31+G(d)		exp. (soln)[48]		B3LYP/6-31+G(d)		exp. (soln)[49]	
sym.	ω	int.	ω	int.	ω	int.	ω	int.	ω	int.
b_{3g}	2227.28	0	2219.69	0			2161.50	0		
b_{2u}	2227.22	6.03	2219.64	6.23	2213	strong	2161.62	179.91	2172	weak
a_g	2242.65	0	2234.83	0			2196.82	0		
b_{1u}	2246.40	0.36	2238.68	1.31	2227	weak	2193.16	437.70	2194	strong

Table 3. Vibrational Frequencies ω (cm^{-1}) (Scaled by 0.9614) and Intensities (km/mol) for the C≡N Stretching Modes of F_4-TCNQ in the Charge-Transfer Complexes Calculated at the B3LYP-D/6-31+G(d) Level

	F_4-TCNQ/4T(1)			F_4-TCNQ/4(3-ET)			F_4-TCNQ/4(3-OET)		
sym.	ω	int.	$\Delta\omega$[a]	ω	int.	$\Delta\omega$	ω	int.	$\Delta\omega$
b_{3g}	2205.30	11.29	14	2197.15	20.02	23	2189.86	47.53	30
b_{2u}	2206.08	12.09	14	2200.26	20.27	19	2193.02	33.17	27
a_g	2224.87	85.54	10	2218.74	112.61	16	2213.52	267.49	21
b_{1u}	2228.02	119.89	11	2222.53	156.45	16	2218.71	135.06	20
	F_4-TCNQ/5T			F_4-TCNQ/6T			F_4-TCNQ/TDATA		
sym.	ω	int.	$\Delta\omega$	ω	int.	$\Delta\omega$	ω	int.	$\Delta\omega$
b_{3g}	2200.89	24.60	18	2201.28	4.67	18	2177.72	33.19	42
b_{2u}	2201.20	20.75	18	2201.39	28.79	18	2185.47	35.14	34
a_g	2219.85	131.63	15	2220.47	116.94	14	2203.26	235.68	32
b_{1u}	2223.89	70.76	15	2224.16	152.79	15	2210.64	286.05	28

[a]The red-shift, $\Delta\omega$, is with respect to the isolated neutral F_4-TCNQ molecule.

dx.doi.org/10.1021/cm201798x|*Chem. Mater.* 2011, 23, 5149−5159

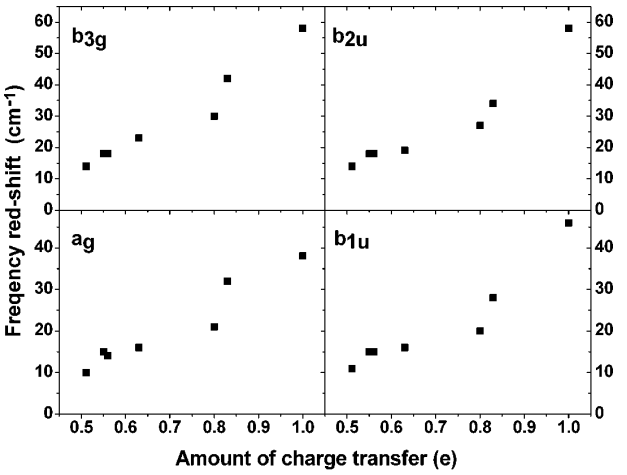

Figure 5. Evolution of the C≡N frequency red-shifts with increasing charge transfer in F_4-TCNQ complexes. Data points for the isolated F_4-TCNQ anion are also shown. Each panel is for a different stretching mode. Red-shifts are with respect to the isolated neutral molecule.

(*Pbca* space group with the unit cell parameters a = 14.678, b = 9.337, and c = 8.174 Å).[51] The unit cell comprises four molecules, each at an inversion center, and gives rise to a total of 16 C≡N stretching modes (see Table 4); the five IR-active

Table 4. Vibrational Frequencies ω (cm^{-1}) (Scaled by 0.9614) and Intensities (km/mol) for the C≡N Stretching Modes in the Pristine F_4-TCNQ Crystal Calculated at the B3LYP/6-31G(d) Level

crystal			solid film (exp.)[c]		
sym.[a]	ω	int.	sym.[b]	ω	int.
A_u	2235.03	0	b_{2u}	2214	weak
B_{2u}	2235.07	0			
B_{1u}	2235.56	45.27			
B_{3u}	2235.43	16.25			
B_{3g}	2235.49	0	b_{3g}		
B_{1g}	2235.36	0			
B_{2g}	2235.83	0			
A_g	2235.84	0			
B_{3g}	2250.74	0	a_g		
B_{2g}	2250.82	0			
A_g	2250.98	0			
B_{1g}	2251.26	0			
B_{2u}	2252.49	532.61	b_{1u}	2227	strong
B_{3u}	2252.52	10.76			
A_u	2253.21	0			
B_{1u}	2254.87	669.61			

[a]Capital letters are used to distinguish the crystal from the isolated molecule and complexes. [b]Corresponding symmetries of the isolated F_4-TCNQ molecule. [c]From Pingel et al.[52]

modes out of the 16 modes form two bands, one at about 2235 cm^{-1} (weak) and the other at 2252−2255 cm^{-1} (strong), as calculated at the B3LYP/6-31G(d) level. By comparing to the vibrational modes of the isolated molecule, we find that the weak and strong bands correspond to the b_{2u} and b_{1u} modes, respectively. The fact that the relative intensities are reversed in the solid state vs the isolated molecule, as illustrated again in Figure 6 in the form of a simulated IR spectrum, is in excellent

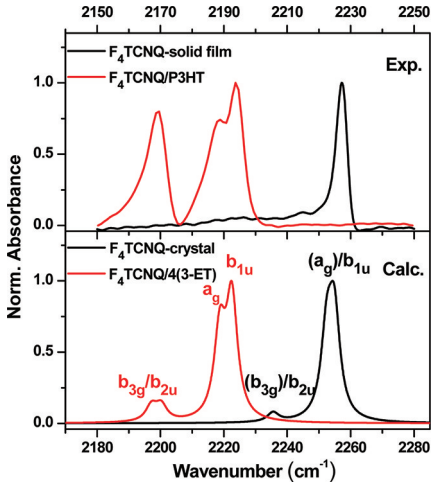

Figure 6. Simulated IR spectra of the C≡N stretching modes for the pristine F_4-TCNQ crystal and the F_4-TCNQ/4(3-ET) complex. The IR-inactive modes (in parentheses) are also given in the labeling of the peaks. A fwhm of 4.5 cm^{-1} was used in the simulations. Experimental spectra for pristine F_4-TCNQ[52] and F_4-TCNQ-doped P3HT[52] are also shown for comparison.

agreement with the experimental results on solid films of F_4-TCNQ.[52]

Comparison of the crystal frequencies to those of the isolated neutral molecule reveals that there is a nearly rigid blue-shift of about 15 cm^{-1} for all calculated crystal frequencies with respect to the isolated molecule. Experimentally, no gas phase data are available for comparison (solution data show[52] no frequency shift), but experimental data on other CN-containing compounds indicate that a gas-to-solid phase change does not appear to cause any frequency shifts.[53] We relate the likely sources of this discrepancy (that add to the stiffening of the bonds) to the slightly smaller basis sets (no diffuse functions) and the absence of the attractive part of dispersion interactions (no dispersion corrections) considered in the crystal calculations. We note that reducing the basis set size from 6-31+G(d) to 6-31G(d) blue-shifts the frequencies by 8 cm^{-1} in the case of the isolated molecule (see Table 2). (It is useful to recall at this stage that the use of diffuse functions can be problematic in the calculation of a periodic system because undesirable effects can occur due to the basis set linear dependence in tightly packed molecular arrangements.[54]) Without losing the generality of our theoretical approach here, we will then use the 6-31+G(d) frequencies of the isolated molecule, not of the crystal, as the reference when evaluating the frequency shifts upon charge transfer.

With increasing chain length of the donor, as shown in Table 3 for thiophene oligomers, the red-shift of the F_4-TCNQ nitrile stretching modes saturates at the level of the five-ring oligomer (5T). This localization/saturation of charge transfer is consistent with a recent experimental observation[52] made in doping homo- (P3HT) and copolymers of 3-hexylthiophene with varying lengths of the thiophene blocks. The extra experimental peak that only appears in the doped (co)polymers about 6 cm^{-1} below the b_{1u} peak is also very well reproduced in the calculations, which enables assignment of this peak to the a_g mode that has gained IR intensity[52] (see Table 3 and Figure 6).

We note that the calculated red-shifts of 23/19 (b_{3g}/b_{2u}), 16 (a_g), and 16 (b_{1u}) cm^{-1} for F_4-TCNQ/4(3-ET) are smaller than the respective experimental values of 45, 39, and 33 cm^{-1}

dx.doi.org/10.1021/cm201798x|*Chem. Mater.* 2011, 23, 5149–5159

for the doped 3HT (co)polymers. To assess the effects of having longer alkyl groups and a longer thiophene backbone, we calculate the IP of 5(3-HT), 5T with hexyls or the hexamer of P3HT, without calculating its complex with F_4-TCNQ. The calculated IP, as will be discussed further later, would only increase the red-shifts to an extent that do not exceed those of 4(3-OET) (see Table 3); with those of 4(3-OET) as the upper limit, the calculated red-shifts are still 13−18 cm^{-1} short of the experimental values. We therefore attribute the discrepancy to the intermolecular effects that a single donor molecule cannot fully account for in our dimer approach. In fact, a similar observation was made by Bloch and co-workers in their original experimental work that the red-shift can be off the linearity by as much as 12 cm^{-1} for TCNQ, depending on the type of the donor at a given amount of charge transfer.[50] The sharp change of 7−12 cm^{-1} with an increment of only 0.03e in charge transfer (compare 4(3-OET) with TDATA as the donor in Table 3 and Figure 5) is also an indication of how sensitive the red-shifts can be to the surrounding environment for a given charged state of the acceptor.

F_4-TCNQ/TDATA is another excellent example that allows us to test our theoretical approach and at the same time to better understand the experimental vibrational spectra. The calculated C≡N stretching frequencies are 2178/2185 (b_{3g}/b_{2u}) cm^{-1} and 2203/2211 (a_g/b_{1u}) cm^{-1} (see Table 3). Experimentally, there are only two bands, one peak at 2171 cm^{-1} and the other at 2192 cm^{-1} (see Figure 7 for a comparison of the experimental and simulated spectra).[55] The 2171 cm^{-1} band can be assigned to b_{3g}/b_{2u}, as was done for the doped thiophene (co)polymers. Considering that there exists only one narrow band around 2192 cm^{-1} that could correspond to a_g and/or b_{1u}, we assign this band to a_g, rather than to b_{1u} or to both modes combined (the assignment in the original experimental work was made to b_{1u}). The reason for this assignment comes from the fact that the experimental IR spectrum was obtained on a heavily doped solid film with a 1:1 molecular ratio. The experimental work on the doping of thiophene (co)polymers by F_4-TCNQ showed[52] that the peak intensity of the b_{1u} mode can become so weak at high dopant concentrations that it can even disappear, leaving a_g alone, all without affecting the band frequencies. The suppression of the b_{1u} intensity is in line with our earlier finding that the peak intensity of b_{1u} is sensitive to intermolecular interactions, which are not fully taken into account in our dimer approach.

With the new assignment, the calculated red-shifts of 42/34 (b_{3g}/b_{2u}) and 32 (a_g) cm^{-1} compare very well with the experimental values of 43 and 36 cm^{-1}, respectively (the IR-inactive a_g frequency of 2228 cm^{-1} for the pristine state is taken from the Raman spectroscopy of a pristine powder[49]). The high level of agreement with the experiment, which was not achieved for the complex with P3HT, is attributed to the larger size and three-dimensional shape of the TDATA molecule that could minimize the missing condensed-phase effects more effectively than the one-dimensional shape of an oligothiophene molecule (see Figures 2 and 7 for comparison of their spatial extent). The calculated charge transfer of 0.83e, which is the highest calculated in our study, is consistent with a recent experimental demonstration of doping TDATA with F_4-TCNQ into a hole-transport layer material with improved injection and transport.[56]

Before leaving this subsection, we stress that it is the frequencies, not the complex geometry or the amount of charge transfer, that are prone to variance as a result of the missing "secondary" intermolecular interactions (if we consider the donor molecule as the "primary" source of the intermolecular interactions, which also determines the amount of charge transfer).

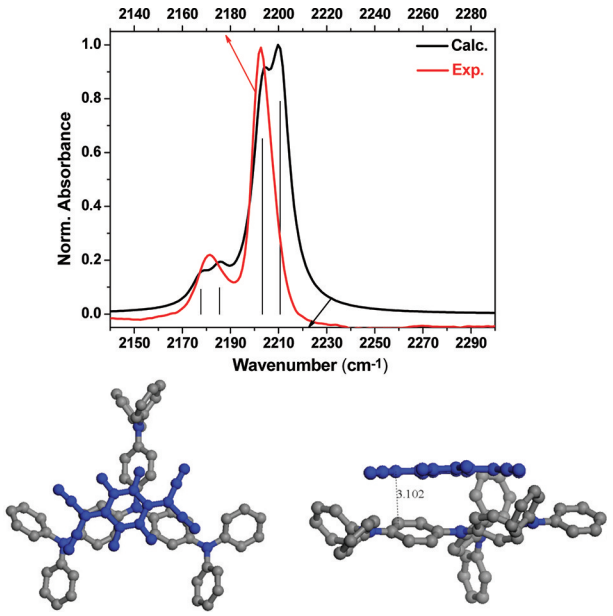

Figure 7. Simulated IR spectrum for the C≡N stretching modes in F_4-TCNQ/TDATA. The vertical lines denote the calculated frequencies with their normalized intensities. A fwhm of 8 cm^{-1} was used in the simulation. The experimental spectrum measured on a F_4-TCNQ/TDATA solid film[55] is reproduced for comparison (in red). The snapshots of the complex structure from two different directions are shown in the bottom panel.

3.4. Offset between the Donor IP and the Acceptor EA. The original charge transfer literature identified the difference between the donor IP and the acceptor |EA| as the most important parameter in understanding the charge-transfer process in molecular complexes.[5] Although the same IP−|EA| offset has been used as a working principle in doping research, the |EA| of the dopant is, more often than not, greater than the IP of the semiconductor if any doping action is to be effected.[1] By using molecules considered here as an example, it is observed that, in the solid state, the |EA| of F_4-TCNQ, 5.24 eV from inverse photoelectron spectroscopy (IPES),[57] is greater than the IP of TDATA, 4.65 eV from ultraviolet photoelectron spectroscopy (UPS)[55] (see Table 5 for some other donors). It is important to realize, however, that the difference IP − |EA| reverses its sign to positive when solid-state effects are removed, as seen from comparison with the gas-phase data. In fact, such a reversal is quite general. Taking into account a solid-state electronic polarization energy for holes (or the difference between the gas-phase and solid-state IPs) of about 1.6 eV common for many organic molecules[58] and assuming the same value for electrons, it can be realized that for a *p*-dopant with |EA| greater than the donor IP by as much as 3 eV in the solid state, a positive IP − |EA| could still be found in the gas phase.

DFT values of the single-molecule IP and EA for some of the compounds are collected in Table 5, along with experimental gas-phase results. Studies have shown[59,62−64] that the values of vertical IP/EA, calculated in a self-consistent way by removing/adding an electron from/to the molecule, compare well with the measurements of photoelectron spectroscopy but that such an agreement progressively deteriorates with increasing

dx.doi.org/10.1021/cm201798x|*Chem. Mater.* 2011, 23, 5149−5159

Table 5. Single-Molecule Ionization Potentials (IP) and Electron Affinities (EA) Calculated at the B3LYP/6-31+G(d) Level

	IP of the donor (eV)			EA of F_4-TCNQ (eV)		
donor	vertical	Koopmans' [a]	exp.	vertical	Koopmans' [b]	exp.
4T	6.45	5.18	7.17[c]	−4.03	−5.54	−3.22[f] (−5.24)[g]
5T	6.14	5.00				
6T	5.96	4.93	6.96[c] (5.3)[d]			
TDATA	5.49	4.59	(4.65)[e]			

[a]Negative of the HOMO energy. [b]LUMO energy. [c]Gas-phase UPS.[59] [d]Solid-state UPS.[60] [e]Solid-state UPS.[55] [f]Gas-phase value estimated from an electrochemical measurement in solution.[61] [g]Solid-state IPES.[57]

molecular size, as a result of the self-interaction errors of commonly used DFT functionals that tend to over-delocalize the extra charge.[65] In the particular case of oligothiophenes, the self-interaction errors can become very visible at six rings (6T).[62] On the other hand, the IP and EA values derived from Koopmans' theorem[66] (that is, the negative of the HOMO (highest occupied molecular orbital) energy and the LUMO (lowest unoccupied MO) energy) have been shown to describe a wide variety of molecules in the *solid state* extremely well (at the B3LYP level);[60] in other words, the −HOMO and LUMO energies can be directly compared in a practical way with the solid-state UPS and IPES values, respectively. This proves particularly useful for F_4-TCNQ (Koopmans' vs solid-state = −5.54 vs −5.24 eV) and TDATA (4.59 vs 4.65 eV), for which gas-phase experimental data are either indirectly obtained or unavailable (Table 5). Here, we define the "gas-phase" IP and |EA| values, in eV, as |(HOMO energy) − 1.6| and |(LUMO energy) + 1.6|, respectively, where the adjustment by 1.6 eV is simply the common experimental value of the solid-state electronic polarization energy. Note that we will use this definition for the remainder of our discussion unless otherwise stated.

The electronic structure of a charge-transfer complex is illustrated in Figure 8 in the case of F_4-TCNQ/4T. For the

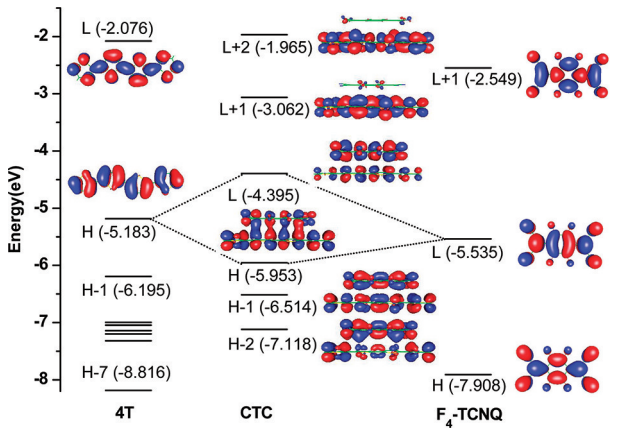

Figure 8. Molecular orbital energy level diagram for F_4-TCNQ/4T(1) before and after formation of the charge-transfer complex. The complex and isolated molecules are calculated at the B3LYP-D/6-31+G(d) and B3LYP/6-31+G(d) levels, respectively.

systems studied here, the HOMO and LUMO of the complex comprise a mixture of the HOMO of the donor and the LUMO of the acceptor. Experimentally, the formation of a charge-transfer complex can be easily detected by the appearance of additional absorption bands in the near-infrared region that are not shown by either component.[67]

Figure 9 shows the simulated absorption spectra obtained from TDDFT results for F_4-TCNQ/4T(1). In the isolated

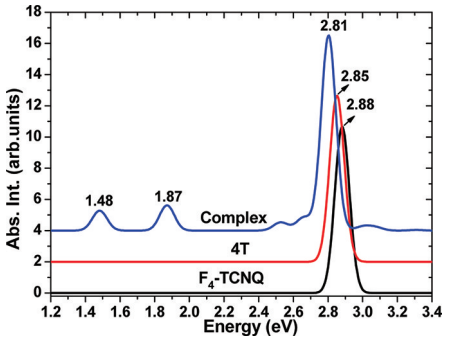

Figure 9. Simulated absorption spectra of F_4-TCNQ/4T(1) obtained from TDDFT results at the B3LYP/6-31+G(d) level.

neutral state, the $S_0 \rightarrow S_1$ transition in 4T appears at 2.85 eV and the lowest-energy transition in F_4-TCNQ is to the S_2 state ($a_g \rightarrow b_{1u}$) at 2.88 eV with the transition to S_1 ($a_g \rightarrow b_{3g}$) being forbidden; both correspond mainly to HOMO-to-LUMO transitions (see Figure 10 for the corresponding natural

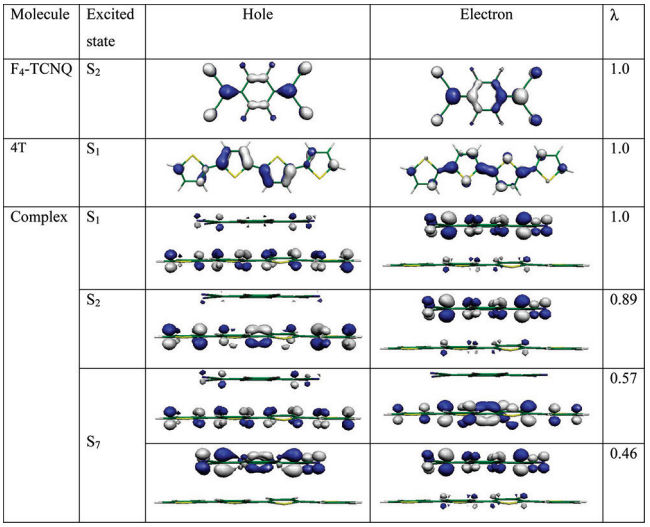

Figure 10. Natural transition orbitals for some lowest excited states calculated by TDDFT at the B3LYP/6-31+G(d) level. The λ value refers to the fraction of the NTO pair contribution to a given electronic excitation.

transition orbitals). The experimental absorption maximum is found at 3.18 eV (390 nm) for 4T in dichloromethane,[68] and a broad absorption peak is measured at about 3.10 eV (400 nm) for F_4-TCNQ in toluene.[7]

dx.doi.org/10.1021/cm201798x|*Chem. Mater.* 2011, 23, 5149–5159

Upon formation of the complex, two new peaks are calculated to appear in the visible-infrared region, one at 1.48 eV (838 nm) and the other at 1.87 eV (663 nm), whereas a third peak is found at 2.81 eV (441 nm) near those of the neutral isolated molecules. The first two transitions are *inter*molecular in nature and a signature of the charge-transfer state; the S_1 transition is predominantly from the donor HOMO to the acceptor LUMO, and the S_2 transition from the donor HOMO−1 to the acceptor LUMO (see Figure 10). The third and strongest transition (S_7) is *intra*molecular and is dominated by the HOMO-to-LUMO transitions of the individual molecules.

The TDDFT results for F_4-TCNQ/4T capture very well the essential features of the charge-transfer state[69] as manifested in the experimental optical absorption spectra of the F_4-TCNQ-doped P3HT film;[7] in the latter, two additional peaks appear at 1.55 eV (880 nm) and 1.61 eV (770 nm). The difference between the two low-energy peaks, which provides a rough measure of the energy gap between the HOMO and HOMO−1 of the donor, is much larger in the calculation (0.39 eV vs 0.06 eV), and is due to the narrowing of this gap with increasing oligomer length. Improved agreement is already seen in going to F_4-TCNQ/5(3-ET), for which the difference between S_1 (1.35 eV) and S_2 (1.65 eV) reduces to 0.3 eV.

So far, we have implicitly assumed that all donor−acceptor pairs in our study are in the strong electronic coupling regime, where a continuous partial charge transfer is to take place.[9] Calculated values of the effective transfer integral t_{eff} between the donor HOMO and the acceptor LUMO, collected in Table 6,

Table 6. Values of the Effective Transfer Integral (Electronic Coupling), t_{eff}, between the HOMO of the Donor and the LUMO of F_4-TCNQ and the Amount of Charge Transfer for All Complexes Calculated at the B3LYP/6-31+G(d) Level

complex	t_{eff} (meV)	CT (e)
F_4-TCNQ/4T	693	0.51
F_4-TCNQ/5T	650	0.55
F_4-TCNQ/6T	624	0.56
F_4-TCNQ/4(3-ET)	719	0.63
F_4-TCNQ/5(3-ET)	666	0.69
F_4-TCNQ/4(3-OET)	701	0.80
F_4-TCNQ/TDATA	389	0.83

indicate that the electronic coupling is indeed strong for all pairs (t_{eff} ∼ 0.4−0.7 eV). We note that the amount of charge transfer does not simply follow the strength of the electronic coupling; for example, TDATA, which transfers the largest amount of charge among all donors, exhibits the smallest t_{eff} (390 meV for TDATA vs 620 to 720 meV for the other molecules). As discussed in more detail below, this suggests that in the strong coupling regime the electronic coupling plays a rather minor role in determining the exact amount of charge transfer.

Plotted in Figure 11 is the amount of partial charge transferred to F_4-TCNQ from the donor as the donor IP approaches the acceptor |EA|. As we noted earlier, the IP−|EA| offset calculated for the isolated molecules is positive for all complexes. Overall, the amount of charge transfer increases with decreasing offset, but clearly, the trend is far from being consistent with the results of Toher et al.[9] In their study on the use of self-interaction corrections to effectively mend the mono-

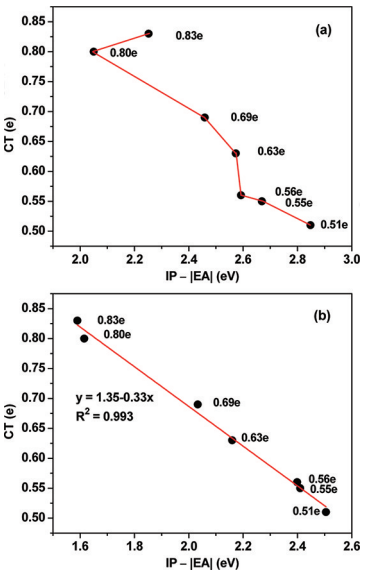

Figure 11. Charge transfer as a function of the offset of the donor IP with respect to the |EA| of F_4-TCNQ. The IPs and EAs, calculated at the B3LYP/6-31+G(d) level, are obtained using (a) the isolated-molecule geometries; and (b) the optimized geometries of the complexes. The lines connecting data points in (a) are for viewing purposes only, while the straight line in (b) is a result of data fitting. In the order of increasing CT amount, the complexes reported here are those between the acceptor F_4-TCNQ and the donors 4T, 5T, 6T, 4(3-ET), 5(3-ET), 4(3-OET), and TDATA, respectively.

determinantal issue of DFT, Toher et al. showed that, in the strong coupling limit, self-interaction-corrected DFT predicts a charge transfer vs IP − |EA| curve that is very close to what standard DFT calculates in the high charge-transfer range, namely, a nearly straight line irrespective of the strength of electronic coupling.[8,9]

At this stage, it is important to realize that the fact that the amount of charge transfer turns out not to be a monotonically varying function of the IP−|EA| offset has a somewhat distressing implication. This indeed suggests that matching up a host material and a dopant based on their IP and EA values, a common practice in doping research, might not produce doping effects as desired. For instance, among the hole-transport materials we study, the doping effect is less pronounced for 4(3-OET) than for TDATA despite the former having a more favorable IP−|EA| offset (see Figure 11a).

Importantly, however, when the IPs of the donor molecules and the EA of F_4-TCNQ are calculated using the molecular geometries taken out of the *optimized complexes* (consider a two-step process where the donor and acceptor molecules undergo full geometric changes upon forming a complex and then exchange partial charge), instead of those of the optimized *isolated molecules*, we find that, remarkably, all data points in the resulting CT vs IP − |EA| plot fall onto a straight line (see Figure 11b). A linear regression gives

$$\mathrm{CT} = -0.33(\mathrm{IP} - |\mathrm{EA}|) + 1.35 \qquad (2)$$

where CT is in e and IP and EA are in eV. The same level of linearity is also achieved when the vertical IPs and EA, calculated self-consistently, are obtained on such geometries (CT = −0.28(IP − |EA|) + 1.08).

To shed light on the linear dependence of CT on IP − |EA|, we derive below the amount of charge transfer within the

dx.doi.org/10.1021/cm201798x|*Chem. Mater.* 2011, 23, 5149−5159

formalism of the electronic chemical potential and hardness by Parr and Pearson.[70] The formal and operational definitions of the electronic chemical potential μ and the absolute hardness η for an N-electron system with total energy $E(N)$ and nuclear charge Z are given by

$$\mu = \left(\frac{\partial E}{\partial N}\right)_Z = -\frac{\mathrm{IP} + |\mathrm{EA}|}{2} = -\chi \tag{3}$$

$$\eta = \frac{1}{2}\left(\frac{\partial^2 E}{\partial N^2}\right)_Z = \frac{\mathrm{IP} - |\mathrm{EA}|}{2} \tag{4}$$

where χ is the absolute electronegativity of Mulliken.[71] We can write the electronic chemical potentials for the donor D and the acceptor A after charge transfer as

$$\mu_A = \mu_A^0 + 2\eta_A \mathrm{CT}$$

$$\mu_D = \mu_D^0 - 2\eta_D \mathrm{CT}$$

where μ^0 and η are those of the isolated molecules in their complex geometries. Equalization of the chemical potentials upon complex formation leads to

$$\mathrm{CT} = \frac{\chi_A^0 - \chi_D^0}{2(\eta_A + \eta_D)} \tag{5}$$

Before making further use of eq 5 for our discussion, we confirm its validity by plotting CT estimated from eq 5, $\mathrm{CT_{PP}}$, against CT obtained directly from the population analysis, $\mathrm{CT_{pop}}$. The comparison is shown in Figure 12.

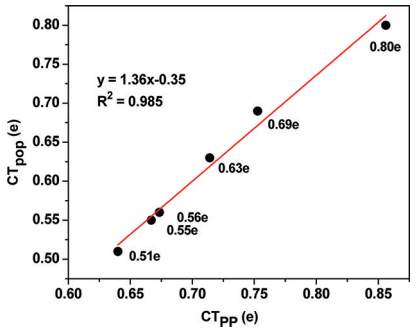

Figure 12. Charge transfer estimated by eq 5, $\mathrm{CT_{PP}}$, in comparison to that of the population analysis, $\mathrm{CT_{pop}}$. The IPs and EAs (|HOMO|s and LUMOs), calculated at the B3LYP/6-31+G(d) level, are those obtained using the optimized geometries of the complexes. The straight line is the result of data fitting. The complexes reported here are the same as in Figure 11, except that the data point for TDATA is not shown (for which the LUMO energy of −0.85 eV is too high to form a stable anion).

Using eqs 3 and 4, we can rewrite eq 5 as

$$\mathrm{CT} = -\frac{1}{2(\eta_A + \eta_D)}(\mathrm{IP_D} - |\mathrm{EA_A}|) + 0.5 \tag{6}$$

A close examination of eq 6 shows that the linearity between CT and IP − |EA| holds only when $\eta_A + \eta_D$ is constant. We recall that the linear relationship reported by Toher et al.[9] was obtained when an external electric field was applied (to produce the needed variation of the IP−|EA| offset) to a single system at a frozen geometry. The donor−acceptor model of Toher et al. satisfies the linearity condition of eq 6, because $2(\eta_A + \eta_D)$ is simply the sum of the energy gaps of one donor and one acceptor and the energy gaps are not affected by the varying electric field. This linearity condition, however, is not fulfilled in our case where there are multiple donor molecules and they all have different energy gaps; it is clear that the linearity we report among a variety of donor molecules has an origin different from those of the common frozen geometry−electric field models.

We stress here that although the derivation of eq 5 is formally identical to that of Parr and Pearson,[70] their original formulation was presented as a first-order approximation, in which the donor and the acceptor were considered in the geometries of the respective isolated molecules. Using the IPs and EA calculated from the isolated-molecule geometries instead, we observe neither a one-to-one correspondence as seen in Figure 12 between $\mathrm{CT_{PP}}$ and $\mathrm{CT_{pop}}$, nor a systematic evolution of CT with respect to IP − |EA| (results not shown).

To summarize the key findings of this subsection, we have established a general relationship between the amount of charge transfer and the IP−|EA| offset in strongly coupled systems, by showing that the linearity of this relationship holds among diverse doped systems and that the relevant IP−|EA| offset is the "in situ" offset that is determined by the complex geometry, not the offset defined by the individual molecules or materials. We expect that our results remain valid for actual solid-state scenarios, by noting the experimental observation that charge transfer to F_4-TCNQ from thiophene (co)polymer matrices is determined solely by the local IP as defined by a chain segment of 4−5 thiophene rings, which is independent of the composition of the segment's immediate surroundings.[52] From the fact that among many chain segments surrounding a particular dopant molecule, there is only one segment of finite size that actually acts as a donor, we also expect that our dimer approach is equally applicable to dopants of any size. An important implication of these results from a practical point of view is that the use of the intrinsic IP and EA values alone, whether determined in the gas phase or the solid state, or whether theoretical or experimental, could fail to predict the doping effect even at a qualitative level.

4. CONCLUSIONS

We have theoretically investigated the charge-transfer process in the *p*-doping by F_4-TCNQ of seven hole-transport molecules of varying IPs, using dispersion-corrected DFT methods. By calculating the fully optimized geometries of their charge-transfer complexes, we established a relationship between the amount of charge transfer and the offset between the donor IP and the acceptor EA, IP − |EA|, in the strong electronic coupling regime.

Importantly, the amount of charge transfer among various complexes is not a monotonic function of IP − |EA|, which contrasts with the commonly held views found in experimental studies and earlier predictions based on simple theoretical models. Linearity emerges, however, when the IP and EA values are adjusted to reflect the *intra*molecular geometric changes upon formation of the complex. The resulting offset represents what would be the IP−|EA| offset measured in situ within the fully relaxed complex, yet without charge transfer.

The intermolecular complex geometries were shown to be impacted greatly by the dispersion interactions but to be nearly unaffected by the varying IP−|EA| offset once proper dispersion interactions are put in place. While the (static) bond-length

dx.doi.org/10.1021/cm201798x | *Chem. Mater.* 2011, 23, 5149–5159

changes upon complex formation are dictated by the amount of charge transfer alone, the frequency red-shifts of the C≡N stretching modes in F_4-TCNQ, a common experimental marker for charge transfer, were found to be sensitive to the intermolecular environment as well.

Our results, obtained with the mono-determinantal DFT approach, are valid within the confines of strong coupling and high charge-transfer limits. These are the conditions expected to be encountered most often in molecular doping. Thus, our study provides a practical tool, based on straightforward theoretical calculations as described above, to find donor−acceptor pairs for desired doping effects and to estimate the resulting charge density in organic semiconductors.

■ ASSOCIATED CONTENT

Ⓢ Supporting Information

Complete ref 28. This material is available free of charge via the Internet at http://pubs.acs.org.

■ AUTHOR INFORMATION

Corresponding Authors

*E-mail: eg.kim@dankook.ac.kr; jean-luc.bredas@chemistry.gatech.edu.

Present Addresses

[†]Department of Polymer Science and Engineering, Dankook University, Jukjeon, Gyeonggi 448−701, Korea.

[‡]Department of Chemistry, King Abdulaziz University, Jeddah 21589, Saudi Arabia.

■ ACKNOWLEDGMENTS

We acknowledge stimulating discussions with Drs. Veaceslav Coropceanu, Hong Li, and John Sears at Georgia Tech and Prof. Norbert Koch at Humboldt University Berlin. This work was partly supported by the Department of Energy (DE-FG02-04ER46165) and Solvay.

■ REFERENCES

(1) Walzer, K.; Maennig, B.; Pfeiffer, M.; Leo, K. *Chem. Rev.* **2007**, *107*, 1233.

(2) Koch, N. *ChemPhysChem* **2007**, *8*, 1438.

(3) Chan, C. K.; Zhao, W.; Kahn, A.; Hill, I. G. *Appl. Phys. Lett.* **2009**, *94*, 203306.

(4) Mulliken, R. S.; Person, W. B. *Annu. Rev. Phys. Chem.* **1962**, *13*, 107.

(5) Bender, C. J. *Chem. Soc. Rev.* **1986**, *15*, 475.

(6) Morokuma, K. *Acc. Chem. Res.* **1977**, *10*, 294.

(7) Yim, K.-H.; Whiting, G. L.; Murphy, C. E.; Halls, J. J. M.; Burroughes, J. H.; Friend, R. H.; Kim, J.-S. *Adv. Mater.* **2008**, *20*, 3319.

(8) Avilov, I.; Geskin, V.; Cornil, J. *Adv. Funct. Mater.* **2009**, *19*, 624.

(9) Toher, C.; Filippetti, A.; Sanvito, S.; Burke, K. *Phys. Rev. Lett.* **2005**, *95*, 146402.

(10) Zhang, Y.; de Boer, B.; Blom, P. W. M. *Adv. Funct. Mater.* **2009**, *19*, 1901.

(11) Gao, Z. Q.; Mi, B. X.; Xu, G. Z.; Wan, Y. Q.; Gong, M. L.; Cheah, K. W.; Chen, C. H. *Chem. Commun.* **2008**, 117.

(12) Garnier, F.; Hajlaoui, R.; Yassar, A.; Srivastava, P. *Science* **1994**, *265*, 1684.

(13) Pfeiffer, M.; Leo, K.; Zhou, X.; Huang, J. S.; Hofmann, M.; Werner, A.; Blochwitz-Nimoth, J. *Org. Electron.* **2003**, *4*, 89.

(14) Huang, J.; Blochwitz-Nimoth, J.; Pfeiffer, M.; Leo, K. *J. Appl. Phys.* **2003**, *93*, 838.

(15) Zhou, Z.; Pfeiffer, M.; Blochwitz, J.; Werner, A.; Nollau, A.; Fritz, T.; Leo, K. *Appl. Phys. Lett.* **2001**, *78*, 410.

(16) Braun, K. F.; Hla, S. W. *J. Chem. Phys.* **2008**, *129*, 064707.

(17) Hwang, J.; Kahn, A. *J. Appl. Phys.* **2005**, *97*, 103705.

(18) Grimme, S. *J. Comput. Chem.* **2004**, *25*, 1463.

(19) Grimme, S. *J. Comput. Chem.* **2006**, *27*, 1787.

(20) Feyereisen, M.; Fitzgerald, G.; Komornicki, A. *Chem. Phys. Lett.* **1993**, *208*, 359.

(21) Scott, A. P.; Radom, L. *J. Phys. Chem.* **1996**, *100*, 16502.

(22) Senthilkumar, K.; Grozema, F. C.; Bichelhaupt, F. M.; Siebbeles, L. D. A. *J. Chem. Phys.* **2003**, *119*, 9809.

(23) Valeev, E. F.; Coropceanu, V.; da Silva Filho, D. A.; Salman, S.; Brédas, J.-L. *J. Am. Chem. Soc.* **2006**, *128*, 9882.

(24) Martin, R. L. *J. Chem. Phys.* **2003**, *118*, 4775.

(25) Dreuw, A.; Head-Gordon, M. *Chem. Rev.* **2005**, *105*, 4009.

(26) *TURBOMOLE 6.0*; TURBOMOLE GmbH: Karlsruhe, Germany, 2009.

(27) Dovesi, R.; Saunders, V. R.; Roetti, C.; Orlando, R.; Zicovich-Wilson, C. M.; Harrison, N. M.; Doll, K.; Civalleri, B.; Bush, I. J.; D'Arco, P.; Llunell, M. *CRYSTAL06*; CRYSTAL Theoretical Chemistry Group: Torino, Italy, 2006.

(28) Frisch, M. J., et al. *Gaussian03*, E.01; Gaussian, Inc.: Wallingford, CT, 2004. Complete reference found in the Supporting Information.

(29) Jurečka, P.; Černý, J.; Hobza, P.; Valdés, H. *J. Comput. Chem.* **2006**, *28*, 555.

(30) Seponer, J.; Leszczynski, J.; Hobza, P. *J. Comput. Chem.* **1996**, *17*, 841.

(31) Zimmerli, U.; Parrinello, M.; Koumoutsakos, P. *J. Chem. Phys.* **2004**, *120*, 2693.

(32) Černý, J.; Jurečka, P.; Hobza, P.; Valdés, H. *J. Phys. Chem. A* **2007**, *111*, 1146.

(33) Wu, Q.; Yang, W. *J. Chem. Phys.* **2002**, *116*, 515.

(34) Hohenstein, E. G.; Chill, S. T.; Sherrill, C. D. *J. Chem. Theory Comput.* **2008**, *4*, 1996.

(35) Grimme, S.; Antony, J.; Ehrlich, S.; Krieg, H. *J. Chem. Phys.* **2010**, *132*, 154104.

(36) Guallar, V.; Borrelli, K. W. *Proc. Natl. Acad. Sci. U.S.A* **2005**, *102*, 3954.

(37) Alber, F.; Kuonen, O.; Scapozza, L.; Folkers, G.; Carloni, P. *Proteins* **1998**, *31*, 453.

(38) Černý, J.; Hobza, P. *Phys. Chem. Chem. Phys.* **2005**, *7*, 1624.

(39) Aziz, E. E.; Vollmer, A.; Eisebitt, S.; Eberhardt, W.; Pingel, P.; Neher, D.; Koch, N. *Adv. Mater.* **2007**, *19*, 3257.

(40) Tsuzuki, S.; Honda, K.; Uchimaru, T.; Mikami, M. *J. Chem. Phys.* **2004**, *120*, 647.

(41) Grimme, S. *Chem.—Eur. J.* **2004**, *10*, 3423.

(42) Kistenmacher, T. J.; Emge, T. J.; Bloch, A. N.; Cowan, D. O. *Acta Crystallogr., Sect. B: Struct. Crystallogr. Cryst. Chem.* **1982**, *38*, 1193.

(43) Coppens, P.; Row, T. N. G. *Ann. N.Y. Acad. Sci.* **1978**, *313*, 244.

(44) Flandrois, S.; Chasseau, D. *Acta Crystallogr., Sect. B: Struct. Commun.* **1977**, *33*, 2744.

(45) Bozio, R.; Pecile, C. In *Spectroscopy of Advanced Materials*; Clark, R. J., Hester, R. E., Eds.; Wiley: New York, 1991.

(46) Maennig, B.; Pfeiffer, M.; Nollau, A.; Zhou, X.; Leo, K. *Phys. Rev. B* **2001**, *64*, 195208.

(47) Stires, J. C.; McLaurin, E. J.; Kubiak, C. P. *Chem. Commun.* **2005**, 3532.

(48) Koch, N. Private communication.

(49) Meneghetti, M.; Pecile, C. *J. Chem. Phys.* **1986**, *84*, 4149.

(50) Chappell, J. S.; Bloch, A. N.; Bryden, W. A.; Maxfield, M.; Poehler, T. O.; Cowan, D. O. *J. Am. Chem. Soc.* **1981**, *103*, 2443.

(51) Emge, T. J.; Maxfield, M.; Cowan, D. O.; Kistenmacher, T. J. *Mol. Cryst. Liq. Cryst.* **1981**, *65*, 161.

(52) Pingel, P.; Zhu, L.; Park, K. S.; Vogel, J.-O.; Janietz, S.; Kim, E.-G.; Rabe, J. P.; Brédas, J.-L.; Koch, N. *J. Phys. Chem. Lett.* **2010**, *1*, 2037.

(53) Cradock, S.; Huntley, C. M.; Rankin, D. W. H. *J. Mol. Struct.* **1988**, *178*, 217.

(54) Towler, M. D. *Proceedings of HCM Network School Hartree−Fock Theory of the Electronic Structure of Solids*, 1995.

(55) Duhm, S.; Salzmann, I.; Broker, B.; Glowatzki, H.; Johnson, R. L.; Koch, N. *Appl. Phys. Lett.* **2009**, *95*, 093305.
(56) Zhou, X.; Blochwitz, J.; Pfeiffer, M.; Nollau, A.; Fritz, T.; Leo, K. *Adv. Funct. Mater.* **2001**, *11*, 310.
(57) Gao, W.; Kahn, A. *Appl. Phys. Lett.* **2001**, *79*, 4040.
(58) Sato, N.; Seki, K.; Inokuchi, H. *J. Chem. Soc., Faraday Trans. 2* **1981**, *77*, 1621.
(59) da Silva Filho, D. A.; Coropceanu, V.; Fichou, D.; Gruhn, N. E.; Bill, T. G.; Gierschner, J.; Cornil, J.; Brédas, J. L. *Philos. Trans. R. Soc., A* **2007**, *365*, 1435.
(60) Djurovich, P. I.; Mayo, E. I.; Forrest, S. R.; Thompson, M. E. *Org. Electron.* **2009**, *10*, 515.
(61) Chen, E. C. M.; Wentworth, W. E. *J. Chem. Phys.* **1975**, *63*, 3183.
(62) Telesca, R.; Bolink, H.; Yunoki, S.; Hadziioannou, G.; Van Duijnen, P. T.; Snijders, J. G.; Jonkman, H. T.; Sawatzky, G. A. *Phys. Rev. B* **2001**, *63*, 155112.
(63) Sánchez-Carrera, R. S.; Coropceanu, V.; da Silva Filho, D. A.; Friedlein, R.; Osikowicz, W.; Murdey, R.; Suess, C.; Salaneck, W. R.; Brédas, J.-L. *J. Phys. Chem. B* **2006**, *110*, 18904.
(64) Kim, E.-G.; Coropceanu, V.; Gruhn, N. E.; Sánchez-Carrera, R. S.; Snoeberger, R.; Matzger, A. J.; Brédas, J.-L. *J. Am. Chem. Soc.* **2007**, *129*, 13072.
(65) Kummel, S.; Kronik, L. *Rev. Mod. Phys.* **2008**, *80*, 3.
(66) We use the term "Koopmans' theorem" loosely here, a common practice to refer to the use of the Kohn−Sham (KS) MO energies for the IP and EA, which, strictly speaking, is misleading or even incorrect because (i) the IP from total energy calculations is not reproduced by the HOMO energy because of the deficiency of common density functionals and (ii) there is no formal KS equivalent of the theorem involving the LUMO.
(67) Lee, J.-H.; Leem, D.-S.; Kim, H.-J.; Kim, J.-J. *App. Phys. Lett.* **2009**, *94*, 123306.
(68) Garcia, P.; Penuut, J. M.; Hapiot, P.; Wiatgens, V.; Vaht, P.; Gander, F.; Dehbouglise, D. *J. Phys. Chem.* **1993**, *97*, 513.
(69) Additional calculations using CAM-B3LYP and ωB97X, two of the so-called long-range-corrected functionals that have been developed specifically to improve the description of charge-transfer excited states, confirm our results with B3LYP, with the charge-transfer excited states calculated to be at higher energies, which is expected from a better description of long-range interactions.
(70) Parr, R. G.; Pearson, R. G. *J. Am. Chem. Soc.* **1983**, *105*, 7512.
(71) Mulliken, R. S. *J. Chem. Phys.* **1934**, *2*, 782.

■ NOTE ADDED AFTER ASAP PUBLICATION

There was an error in section 3.4 in the version published ASAP November 8, 2011; the corrected version published ASAP November 10, 2011.